

Electrical and optical properties of degenerate and semi-insulating ZnGa_2O_4 : Electron/phonon scattering elucidated by quantum magnetoconductivity ^{EP}

Cite as: Appl. Phys. Lett. **116**, 252104 (2020); <https://doi.org/10.1063/5.0014827>

Submitted: 10 April 2020 . Accepted: 06 June 2020 . Published Online: 22 June 2020

David C. Look , Kevin D. Leedy , Ray-Hua Horng , Marco D. Santia, and Stefan C. Badescu

COLLECTIONS

 This paper was selected as an Editor's Pick



View Online



Export Citation



CrossMark

ARTICLES YOU MAY BE INTERESTED IN

[Exfoliated hexagonal BN as gate dielectric for InSb nanowire quantum dots with improved gate hysteresis and charge noise](#)

Applied Physics Letters **116**, 253101 (2020); <https://doi.org/10.1063/5.0002112>

[All-fiber focused beam generator integrated on an optical fiber tip](#)

Applied Physics Letters **116**, 241102 (2020); <https://doi.org/10.1063/5.0007022>

[Different types of band alignment at \$\text{MoS}_2\$ /\(Al, Ga, In\)N heterointerfaces](#)

Applied Physics Letters **116**, 252102 (2020); <https://doi.org/10.1063/5.0009469>

Lock-in Amplifiers
up to 600 MHz



Watch



Electrical and optical properties of degenerate and semi-insulating ZnGa₂O₄: Electron/phonon scattering elucidated by quantum magnetoconductivity

Cite as: Appl. Phys. Lett. **116**, 252104 (2020); doi: 10.1063/5.0014827

Submitted: 10 April 2020 · Accepted: 6 June 2020 ·

Published Online: 22 June 2020



View Online



Export Citation



CrossMark

David C. Look,^{1,2,a)}  Kevin D. Leedy,²  Ray-Hua Horng,³  Marco D. Santia,^{2,4} and Stefan C. Badescu²

AFFILIATIONS

¹Semiconductor Research center, Wright State University, 3640 Colonel Glenn Hwy, Dayton, Ohio 45435, USA

²Air Force Research Laboratory Sensors Directorate, 2241 Avionics Circle, Wright-Patterson AFB, Ohio 45433, USA

³Institute of Electronics, National Chiao Tung University, 1001 University Road, Hsinchu 30010 Taiwan

⁴National Research Council, 2241 Avionics Circle, Wright-Patterson AFB, Ohio 45433, USA

^{a)}Author to whom correspondence should be addressed: david.look@wright.edu

ABSTRACT

We study the electrical and optical properties of degenerate ZnGa₂O₄ films grown by metalorganic chemical vapor deposition (MOCVD) on sapphire and semi-insulating films grown by pulsed laser deposition (PLD) on fused silica. After a forming-gas anneal at 700 °C, the MOCVD film is highly conducting, with a room-temperature carrier concentration of $2 \times 10^{20} \text{ cm}^{-3}$, a mobility of 20 cm²/V s, and direct bandgap absorptions at 3.65 eV and 4.60 eV. Under the same annealing conditions, the PLD film is semi-insulating, with a direct bandgap absorption at 5.25 eV. The phonon structure, important for electrical and thermal conduction as well as superconductivity and other quantum phenomena, is very complicated due to the large number of atoms (and, thus, phonon branches) in the unit cell. However, we show that the phonon contributions to electron mobility (μ_{ph}) can be *directly* measured by quantum-based magnetoconductivity over the temperature span $T = 10\text{--}200$ K. From an approximate analytical formula, $\mu_{\text{ph}} = \text{function}(T_{\text{ph}}, T)$, we calculate an effective phonon energy $kT_{\text{ph}}(T)$ that takes account of *all* phonon contributions at temperature T . For $T = 10\text{--}200$ K, the value of kT_{ph} ranges from about 10 to 90 meV, consistent with the energy range of the ZnGa₂O₄ phonon density of states (at 0 K) calculated by density functional theory. The *total* measured mobility can then be modeled by $\mu_{\text{tot}}^{-1} = \mu_{\text{ii}}^{-1} + \mu_{\text{ph}}^{-1}$, where μ_{ii} is the mobility due to ionized-impurity scattering. With a high bandgap, controllable conductivity, high breakdown voltage, and bulk-growth capability, ZnGa₂O₄ offers opportunities for high-power electronics and UV detectors.

Published under license by AIP Publishing. <https://doi.org/10.1063/5.0014827>

In the past few years, the wide-bandgap semiconductor β -Ga₂O₃ has been challenging SiC and GaN in high-power-electronic and UV-photonics applications, mainly because of its much higher bandgap, higher breakdown voltage, availability in bulk form, and controllable conductivity.^{1–4} More recently, another material, ZnGa₂O₄, has been shown to have similar properties: bulk growth with controllable conductivity,⁵ a high bandgap,^{5–9} and a high breakdown voltage.¹⁰ For example, bulk material, with a bandgap of 4.6 eV, can easily be made semi-insulating; however, it can also be made highly conducting with a carrier concentration of $9 \times 10^{19} \text{ cm}^{-3}$ at a mobility of about 100 cm²/V s.⁵ Additionally, ZnGa₂O₄ has a large advantage over β -Ga₂O₃ in ease of Ohmic-contact formation.¹¹ However, in both

materials, the electron mobility is difficult to model, mainly due to a large number of optical phonons.^{12,13} For example, β -Ga₂O₃ has ten atoms in its unit cell, which means that there are 30 normal-mode phonons (3 acoustic, 27 optical), many of which have strong electron-phonon interactions. Similarly, ZnGa₂O₄ has 14 atoms in the unit cell, generating 39 optical phonons. Thus, the usual simplification of assuming only one dominant optical phonon in the scattering, e.g., as applied to ZnO (72-meV LO phonon) and GaN (93-meV), is not possible. Furthermore, in all highly doped n-type thin films, the donor positions are random, leading to disorder and partial localization of the electrons.^{14,15} Also, the region near the substrate/layer interface will suffer lattice disorder. In such an environment, selection rules are

relaxed and phonon modes are mixed, with even acoustic modes mixing with optical modes. Clearly, the theoretical problems of modeling transport in disordered materials are very challenging. With that in mind, we have introduced a method of investigating phonons.¹⁶ Our approach is to find an *effective* phonon energy kT_{ph} that will correctly represent the *total* electron-phonon scattering at a given temperature T , i.e., $kT_{\text{ph}}(T)$. This method makes use of the wave nature of the electron as it diffuses and scatters among the random donors and other lattice imperfections, a process perhaps best understood through the Feynman approach to quantum mechanics. That is, we can think of the electron wave as being broken into a sum of all possible paths whose amplitudes (not intensities) must be added and then squared to get the final result. Among the various paths, there is a probability that the electron will scatter around a loop of centers, thus returning to the point at which it entered the loop. In such a case, the electron can traverse the loop in either a clockwise or counterclockwise direction, and since the distance is exactly the same, those two paths will interfere constructively at the entry point, thus becoming more probable than random paths containing no loops. Because the motion around a loop essentially moves the electron backward, the resistivity is effectively *increased* over that of a path of similar length with no loops. However, this constructive interference can be reduced or destroyed if the electron phase is changed during the loop traversal, a process that can occur in the presence of a magnetic field or an inelastic scattering event. For the semiconductors of interest here, inelastic phonon scattering is the most important phase-destroying lattice process, although at very low temperatures (say, $T < 5$ K), spin-orbit scattering can also contribute.

These phenomena have been quantified in a 3D theory due to Kawabata,¹⁷ who calculates a term $\Delta\sigma(B, T) = \sigma(B, T) - \sigma(0, T)$, where B is the magnetic-field strength. Kawabata's $\Delta\sigma$ is a *positive* contribution to conductivity, arising from quantum interference, and we will thus call it "quantum magnetoconductivity" (QMC). Note that it competes with the usual classical magnetoconductivity (CMC), a *negative* contribution. (As is well known, the CMC vanishes for a single band of *degenerate* electrons, but can be non-zero if two or more types of electrons are present.¹⁸) For all the materials that we have investigated so far, the QMC is much larger than the CMC at very low temperatures and even up to about 200 K or higher.

Kawabata's result for $\Delta\sigma(B, T)$ is

$$\Delta\sigma(B, T) = \frac{e^2}{2\pi^2\hbar l(B)} \sum_{N=0}^{\infty} 2 \left[(N+1 + \delta(B, T))^{1/2} - (N + \delta(B, T))^{1/2} \right] - \frac{1}{\left(N + \frac{1}{2} + \delta(B, T) \right)^{1/2}}, \quad (1)$$

where

$$\delta(B, T) = \frac{l^2(B)}{4\tau_{\text{ph}}(T)D(T)} = \frac{3e}{4\hbar(3\pi^2n)^{2/3}\mu_{\text{ph}}(T)\mu_{\text{tot}}(T)B}. \quad (2)$$

Here, $D(T)$ is the electron diffusion coefficient, τ_{ph} is the *inelastic* phonon scattering time, and $l(B)$ is a "magnetic length" defined by $l(B) = (\hbar/eB)^{1/2} = 25.656$ nm at $B = 1$ T = 10 kG, the field strength used for most of our measurements. In Eq. (2), we have modified Kawabata's formula by setting $\tau_{\text{ph}} = m^*\mu_{\text{ph}}/e$ and also by invoking the

Einstein relation to get $D = (m^*)(v_f)^2(\mu_{\text{tot}})/3e$, where v_f is the Fermi velocity.¹⁶ It is very helpful that n and μ_{tot} in Eq. (2) can each be *independently* determined in the *same* experiment from measurements of current I , Hall voltage V_H , and B alone. Then, since $\mu_{\text{ph}}(T)$ is the only unknown quantity in Eqs. (1) and (2), it is also determined without knowledge of any other material parameters, putting it on a par with the Hall-effect measurements of n and μ_{tot} . For comparison, in a future work, we will pursue a first-principles calculation of μ_{ph} vs T via density functional theory.

Having established a direct method of measuring μ_{ph} , we seek to relate it to material parameters, and for that, we use the equation

$$\mu_{\text{ph}}(T) = \frac{4\pi\epsilon_0(3/\pi)^{1/3}\hbar^3n^{1/3}T\sinh^2\left(\frac{T_{\text{ph}}}{2T}\right)}{ekT_{\text{ph}}^2(m^*)^2(\epsilon_0/\epsilon_{\infty} - 1)}. \quad (3)$$

This equation has been published elsewhere¹⁶ and is a somewhat modified version of a first-order variational calculation due to Howarth and Sondheimer.¹⁹ For ZnGa_2O_4 , we use the measured value $\epsilon_0 = 9.8$ and estimated values $\epsilon_{\infty} = 3.6$ and $m^* = 0.28m_0$. With these material parameters and the measured values of $\mu_{\text{ph}}(T)$, we can treat Eq. (3) as a transcendental equation and calculate $kT_{\text{ph}}(T)$ from $\mu_{\text{ph}}(T)$.

The total mobility can then be modeled by $\mu_{\text{tot}}^{-1} = \mu_{\text{ii}}^{-1} + \mu_{\text{ph}}^{-1}$, where μ_{ii} is the mobility due to ionized-impurity scattering,^{16,20} given below:

$$\mu_{\text{ii}}(n) = \frac{24\pi^3\epsilon_0^2\hbar^3}{e^3m^{*2}} \frac{1}{\ln(1+y(n)) - \frac{y(n)}{1+y(n)}} \frac{n}{Z^2N_{\text{ii}}} = \mu_{\text{ii0}}(n) \frac{n}{Z^2N_{\text{ii}}}, \quad (4)$$

$$y(n) = \frac{3^{1/3}4\pi^{8/3}\epsilon_0\hbar^2n^{1/3}}{e^2m^*}. \quad (5)$$

For charge $Z=1$, the fit of μ_{tot} vs T yields N_{ii} , the ionized impurity concentration. Then, the relationships $n = N_D - N_A$ and $N_{\text{ii}} = N_D + N_A$, for degenerate electrons, give N_D and N_A , the donor and acceptor concentrations, respectively.²⁰ This is one of the very few ways to determine these quantities. Cases for which Z_D and $Z_A \neq 1$ are illustrated elsewhere.^{16,20}

ZnGa_2O_4 sample #1 was grown at 200 °C by pulsed laser deposition (PLD) as a superlattice: 10-nm ZnO followed by 10-nm Ga_2O_3 , 15 periods, and ≈ 300 nm total thickness. At room temperature (295 K), its resistivity, mobility, and electron concentration were $4.24 \times 10^{-2} \Omega \text{ cm}$, $6.24 \text{ cm}^2/\text{V s}$, and $2.36 \times 10^{19} \text{ cm}^{-3}$, respectively. Reflectance and transmittance measurements were carried out at room temperature using a Perkin-Elmer Lambda 900 UV/Vis/NIR spectrometer over the energy range of 0.38–6.7 eV. Absorption coefficients were calculated by a method that allows both high and low values to be determined, i.e., no approximations are required.²¹ Anneals were performed for 10 min at 500, 600, and 700 °C in a tube furnace under flowing forming gas (FG) consisting of 3% H_2 and 97% Ar. The latter two anneals produced semi-insulating material. Absorption coefficients are plotted in Fig. 1. Here, we have chosen to plot α^2 vs E , rather than the usual $(\alpha E)^2$ vs E (Tauc plots) because the latter holds only for amorphous materials. In fact, our annealed PLD samples are polycrystalline at 600 and 700 °C, with 2-Theta XRD analyses showing

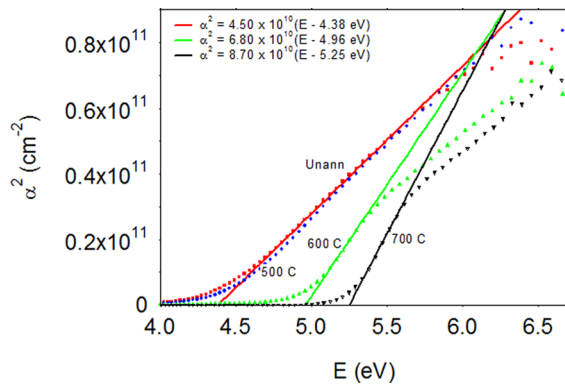


FIG. 1. Plots of α^2 vs E in PLD-grown ZnGa₂O₄ #1, unannealed, and annealed for 10 min in forming gas at 500, 600, and 700 °C, respectively.

only ZnGa₂O₄ with a preferred (111) orientation. Complete structural analysis of the films is beyond the scope of the current work and warrants an additional study. Note that as the sample is annealed up to 700 °C, the bandgap increases to 5.25 eV, among the highest values ever reported for either ZnGa₂O₄ or β -Ga₂O₃.

ZnGa₂O₄ #2 in our study was a 350-nm-thick layer grown at 700 °C by metalorganic chemical vapor deposition (MOCVD) on a c-plane (0001) sapphire (Al₂O₃) substrate; growth details are given elsewhere.^{10,11} At room temperature (295 K), its resistivity, mobility, and electron concentration were $5.60 \times 10^{-3} \Omega \text{ cm}$, $18.1 \text{ cm}^2/\text{V s}$, and $6.16 \times 10^{19} \text{ cm}^{-3}$, respectively. To increase the conductivity, the sample was annealed at 700 °C for 10 min in flowing forming gas (FG), consisting of 3% H₂ and 97% Ar. The resistivity, mobility, and concentration changed to $1.79 \times 10^{-3} \Omega \text{ cm}$, $19.7 \text{ cm}^2/\text{V s}$, and $1.77 \times 10^{20} \text{ cm}^{-3}$, respectively. Temperature-dependent Hall-effect measurements over the range of 13–320 K were carried out in a LakeShore 7507 apparatus at a magnetic field strength of B = 1 T (10 kG). At 13 K, the resistivity, mobility, and concentration were $1.71 \times 10^{-3} \Omega \text{ cm}$, $20.7 \text{ cm}^2/\text{V s}$, and $1.76 \times 10^{20} \text{ cm}^{-3}$, respectively. From these low-temperature results, we calculated donor N_D and acceptor N_A concentrations of $7.87 \times 10^{20} \text{ cm}^{-3}$ and $6.10 \times 10^{20} \text{ cm}^{-3}$, respectively,²⁰ giving a compensation ratio of N_A/N_D = 0.78. This high compensation ratio suggests that the material is not yet optimized and likely can be improved by reducing N_A.

Reflectance and transmittance measurements on ZnGa₂O₄ #2 were carried out at room temperature, and absorption coefficients were calculated as shown in Fig. 2. Unlike the case for ZnGa₂O₄ #1, here, there are two contributions to the bandgap, a small one at 3.45 eV and a larger one at 4.48 eV. The simplest explanation for this observation is that there is a small amount of ZnO phase separation, represented by the 3.45-eV contribution. On the other hand, the XRD showed (hkl) lines associated only with ZnGa₂O₄, and so the fraction of ZnO cannot be too high. This issue will have to be explored further.

Besides the *strong* absorptions shown in Fig. 2, we can also study *weak* absorptions. Note in Fig. 3 that some of the reported deep-center energies⁸ occur near steep increases in α . Since α is quantitative, there is an opportunity to calibrate concentrations of such deep centers, a task to be pursued at a later time.

We now consider the QMC measurements and analysis. We begin by solving $\Delta\sigma_{\text{exp}}(T) = \Delta\sigma_{\text{theo}}(T, B, n, \mu_{\text{tot}}, \mu_{\text{ph}})$, a transcendental

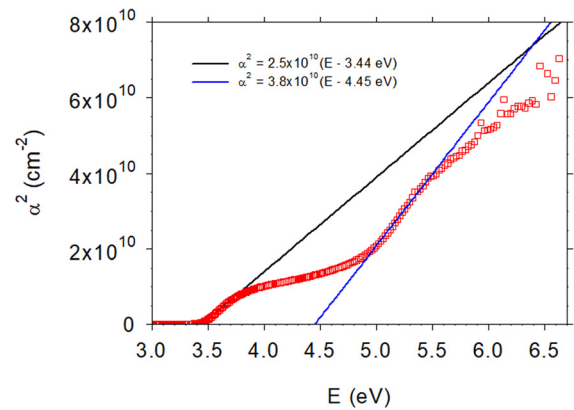


FIG. 2. Plot of α^2 vs E for MOCVD grown ZnGa₂O₄ #2 annealed at 700 °C in forming gas. Note two direct bandgap transitions, at 3.45 and 4.48 eV.

equation, at each value of T, where $\Delta\sigma_{\text{theo}}(T, B, n, \mu_{\text{tot}}, \mu_{\text{ph}})$ consists of Eqs. (1) and (2). The only unknown is μ_{ph} since n and μ_{tot} are measured in the same experiment at the same time by the Hall effect. We employ the “root” function in MathCad²² to solve this equation, but most math programs have a similar function to accomplish this purpose. The solution is the curve $\mu_{\text{ph}}(T)$ vs T, and this is plotted in Fig. 4 as a function of annealing in forming gas at several different temperatures, 500–700 °C. These curves are very robust and repeatable even though $\Delta\sigma/\sigma \leq 0.001$. The solid curves are fits to Eq. (3) and will be discussed below. For comparison, we also plot the measured Hall mobility, $\mu_{\text{tot}} \approx (\mu_{\text{ii}}^{-1} + \mu_{\text{ph}}^{-1})^{-1}$, following an anneal of 700 °C for 10 min. Here, μ_{ii} represents the effects of ionized impurities on the electron scattering, and it is clear that this mechanism totally dominates phonon scattering (since $\mu_{\text{ii}}^{-1} \gg \mu_{\text{ph}}^{-1}$) over the range, T = 10–170 K. (Here, we ignore acoustic-mode deformation potential scattering, calculated from Eq. (4) in Ref. 16 because it contributes only 0.03 and 0.8% of the total scattering at 13 and 300 K,

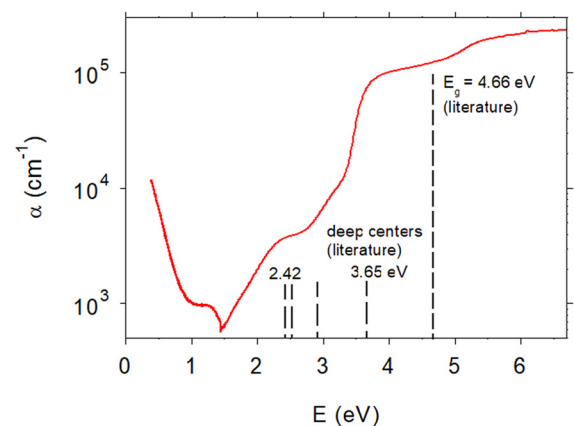


FIG. 3. Absorption coefficient for MOCVD-grown ZnGa₂O₄ #2 compared to representative deep-center and bandgap (E_g) energies (dashed lines) reported in the literature.⁸ (The “cusp” in the data at about 1.4 eV is artificial, due to a detector change in the spectrophotometer.) Note that the thresholds in α correspond roughly to some of the deep-center energies.

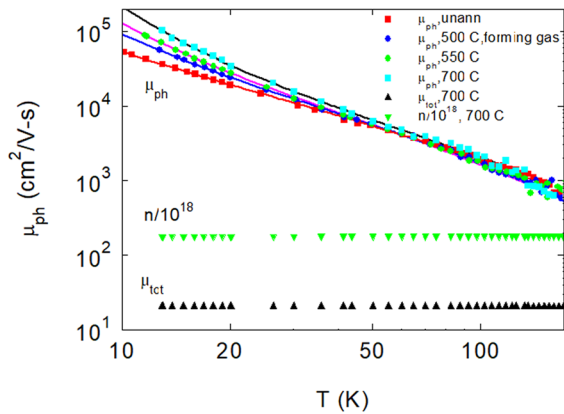


FIG. 4. MOCVD sample #2: determination of μ_{ph} vs T from solving $\Delta\sigma_{\text{theo}}(\mu_{\text{ph}}, T) = \Delta\sigma_{\text{exp}}(T)$ at each value of T , from 13 to 160 K. Various curves represent different annealing temperatures. The measured Hall-effect mobility μ_{tot} and carrier concentration n (in units of cm^{-3}) after a 700 °C anneal are also shown. Note that phonon scattering has very little effect on μ_{tot} since $\mu_{\text{ii}}^{-1} \gg \mu_{\text{ph}}^{-1}$ over the whole temperature range.

respectively.) However, as T increases, phonon scattering always becomes stronger (i.e., μ_{ph}^{-1} increases) and will cause a reduction in μ_{tot} , e.g., at room temperature.

To convert $\mu_{\text{ph}}(T)$ into the effective phonon energy $kT_{\text{ph}}(T)$ at each T , we use Eq. (3). This equation constitutes the first term in a variational calculation¹⁹ and, thus, is only an approximation. In an earlier work,¹⁶ on $\beta\text{-Ga}_2\text{O}_3$, it was thought to be accurate to about 20%. With this limitation in mind, we solve Eq. (3) as a transcendental equation over the range of $T = 13\text{--}160$ K. The results for the unannealed and 500 °C annealed samples are plotted as solid points in Fig. 5, and at the limits of the measurement range, we get $kT_{\text{ph}}(13\text{K}) = 11$ meV and $kT_{\text{ph}}(160\text{K}) = 90$ meV.

One way to check on the reasonableness of these numbers is to calculate the total phonon density of states in the perfect crystal, ignoring disorder from both the random donors and the lattice

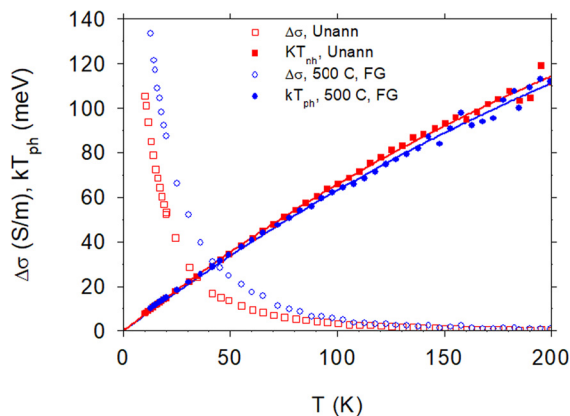


FIG. 5. $\Delta\sigma(B, T) = \sigma(B, T) - \sigma(0, T)$ for MOCVD-grown ZnGa_2O_4 , unannealed, and annealed at 500 °C in forming gas: open points, experimental; closed points, calculations of $\mu_{\text{ph}}(T)$ from Eqs. (1) and (2) and then $kT_{\text{ph}}(T)$ from $\mu_{\text{ph}}(T)$ in Eq. (3).

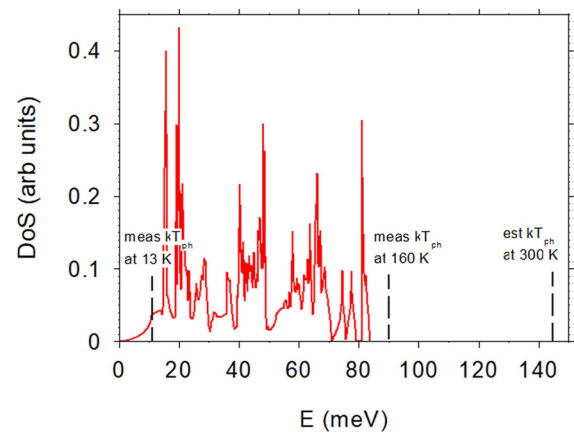


FIG. 6. Theoretical phonon density of states ($T=0$) in single-crystal ZnGa_2O_4 . Also shown are the values of kT_{ph} determined at 13 and 160 K from Fig. 5. Note that the theoretical ($T=0$) and experimental ($T=13\text{--}160$ K) energy spans are quite similar. However, a simple, mathematical extension of the kT_{ph} vs T curve to 295 K is unsuccessful.

mismatch. For that, we use the Quantum Espresso software package²³ that includes density functional theory (DFT) for the lattice structure and density perturbation theory²⁴ for lattice dynamical properties (DFPT). We used ultrasoft pseudopotentials with the PBEsol exchange-correlation potential,²⁵ a plane wave cut-off of 125 Ry and a $16 \times 16 \times 8$ Monkhorst-Pack \mathbf{k} -point grid for structure relaxation with a convergence criterion of 1 mRy/a.u. The Brillouin Zone sampling for lattice dynamical properties consisted of an $8 \times 8 \times 8$ \mathbf{k} -point grid for the electrons and a $4 \times 4 \times 4$ \mathbf{q} -point grid for phonons. The result, at $T=0$, is given in Fig. 6 and is compared with the measured kT_{ph} at 13 and 160 K.

The resulting energy ranges are surprisingly close and suggest that our effective phonon concept has at least a degree of validity. It is then interesting to speculate about extending the kT_{ph} vs T curve to room temperature, 295 K. Indeed, it is easy to fit the curves with an analytical function of the form $kT_{\text{ph}} = a[1 - \exp(-T/b)]$. For example, $a = 264$ meV and $b = 366$ K for the annealed sample, giving $kT_{\text{ph}} = 146$ meV at 295 K, well out of range of the DoS at $T=0$. Of course, we would expect disorder to broaden the DoS, likely moving it to higher energies, but this question will require a more complete theoretical analysis.

In summary, we have studied an emerging semiconductor material, ZnGa_2O_4 , and shown that it competes favorably with another much more widely studied material, $\beta\text{-Ga}_2\text{O}_3$, including having a higher bandgap. Temperature-dependent Hall-effect measurements and analysis yielded donor and acceptor concentrations, and reflectance and transmittance measurements gave both band-to-band and deep-center absorption coefficients. The phonon structure of ZnGa_2O_4 is very complicated due to a large number of atoms in the unit cell. However, we have elucidated the phonon properties using quantum magnetoconductivity measurements and shown reasonable agreement with density functional theory.

This material is based upon the work supported in part by the Air Force Office of Scientific Research under Award No. FA9550-

RY18COR800. Further financial support was provided by the Air Force Research Laboratory under Contract No. FA8075-14-D-0025, the National Science Foundation under Grant No. DMR-1800139 (T. Paskova), the Defense Threat Reduction Agency under Award No. HDTRA1-17-1-0034, and the Ministry of Science and Technology of Taiwan under MOST 108-2218-E-492-010. We wish to thank T. A. Cooper, W. Rice, and D. McFarland for critical technical support in these experiments.

DATA AVAILABILITY

The data that support the findings of this study are available within this article.

REFERENCES

- ¹M. Higashiwaki and G. H. Jessen, "Guest editorial: The dawn of gallium oxide microelectronics," *Appl. Phys. Lett.* **112**, 060401 (2018).
- ²M. Baldini, Z. Galazka, and G. Wagner, *Mater. Sci. Semicond. Process.* **78**, 132 (2018).
- ³A. J. Green, K. D. Chabak, E. R. Heller, R. C. Fitch, Jr., M. Baldini, A. Fiedler, K. Irmscher, G. Wagner, Z. Galazka, S. E. Tetlak, A. Crespo, K. Leedy, and G. H. Jessen, *IEEE Electron Device Lett.* **37**, 902 (2016).
- ⁴K. D. Leedy, K. D. Chabak, V. Vasilyev, D. C. Look, J. J. Boeckl, J. L. Brown, S. E. Tetlak, A. J. Green, N. A. Moser, A. Crespo, D. B. Thomson, R. C. Fitch, J. P. McCandless, and G. H. Jessen, *Appl. Phys. Lett.* **111**, 012103 (2017).
- ⁵Z. Galazka, S. Ganschow, R. Schewski, K. Irmscher, D. Klimm, A. Kwasniewski, M. Pietsch, A. Fiedler, I. Schulze-Jonack, M. Albrecht, T. Schröder, and M. Bickermann, *APL Mater.* **7**, 022512 (2019).
- ⁶P. W. Chen, S. Y. Huang, S. H. Yuan, Y. A. Chen, P. W. Hsiao, and D. S. Wu, *Adv. Mater. Interfaces* **6**, 1901075 (2019).
- ⁷L. L. Noto and M. Mbongo, *Physica B* **578**, 411768 (2020).
- ⁸W. K. Wang, K. F. Liu, P. C. Tsai, Y. J. Xu, and S. Y. Huang, *Coatings* **9**, 859 (2019).
- ⁹E. Chikoidze, C. Sartz, I. Madaci, H. Mohamed, C. Vilar, B. Ballestores, F. Belarri, E. del Corro, P. Vales-Castro, G. Sauthier, L. Li, M. Jennings, V. Sallet, Y. Dumont, and A. Perez-Tomas, *Cryst. Growth Des.* **20**, 2535 (2020).
- ¹⁰L. C. Cheng, C. Y. Huang, and R. H. Horng, *IEEE J. Electron Devices Soc.* **6**, 432 (2018).
- ¹¹Y. S. Shen, W. K. Wang, and R. H. Horng, *IEEE J. Electron Devices Soc.* **5**, 112 (2017).
- ¹²K. Ghosh and U. Singiseti, *Appl. Phys. Lett.* **109**, 072102 (2016).
- ¹³Y. Kang, Y. K. Krishnaswamy, H. Peelaers, and C. G. Van de Walle, *J. Phys.: Condens. Matter* **29**, 234001 (2017).
- ¹⁴P. A. Lee and T. V. Ramakrishnan, *Rev. Mod. Phys.* **57**, 287–337 (1985).
- ¹⁵J. S. Dugdale, *The Electrical Properties of Disordered Metals* (Cambridge University Press, Cambridge, 2005).
- ¹⁶D. C. Look and K. D. Leedy, *Sci. Rep.* **9**, 1290 (2019).
- ¹⁷A. Kawabata, *Solid State Commun.* **34**, 431–432 (1980).
- ¹⁸D. C. Look, *Electrical Characterization of GaAs Materials and Devices* (Wiley, New York, 1989).
- ¹⁹D. J. Howarth and E. H. Sondheimer, *Proc. R. Soc. London, Ser. A* **219**, 53–74 (1953).
- ²⁰D. C. Look, K. D. Leedy, L. Vines, B. G. Svensson, A. Zubiaga, F. Tuomisto, D. R. Douthett, and L. J. Brillson, *Phys. Rev. B* **84**, 115202 (2011).
- ²¹D. C. Look, B. Wang, and K. D. Leedy, *Opt. Eng.* **56**, 034112 (2017).
- ²²PTC, Inc, One Alewife Center, Suite 130, Cambridge, Ma, 02140.
- ²³P. Gianozzi, S. Baroni, N. Bonini, M. Calandra, R. Car, C. Cavazzoni, D. Ceresoli, G. L. Chiarotti, M. Cococcioni, I. Dabo, A. Dal Corso, S. Fabris, G. Fratesi, S. de Gironcoli, R. Gebauer, U. Gerstmann, C. Gougoussis, A. Kokalj, M. Lazzeri, L. Martin-Samos, N. Marzari, F. Mauri, R. Mazzarello, S. Paolini, A. Pasquarello, L. Paulatto, C. Sbraccia, S. Scandolo, G. Sclauzero, A. P. Seitsonen, A. Smogunov, P. Umari, and R. M. Wentzcovitch, *J. Phys.: Condens. Matter* **21**, 395502 (2009).
- ²⁴S. Baroni, S. de Gironcoli, A. Dal Corso, and P. Giannozzi, *Rev. Mod. Phys.* **73**, 515 (2001).
- ²⁵J. P. Perdew, A. Ruzsinszky, G. I. Csonka, O. A. Vydrov, G. E. Scuseria, L. A. Constantin, X. Zhou, and K. Burke, *Phys. Rev. Lett.* **100**, 136406 (2008).